OPTIMAL TAG PATTERN VALIDATION USING MAGNETIC RESONANCE IMAGING

Thomas S. Denney Jr., Jerry L. Prince, Michael J. Lopez, and Elliot R. McVeigh†

Department of Electrical and Computer Engineering
†Department of Biomedical Engineering
Johns Hopkins University , Baltimore, MD 21218, USA

ABSTRACT

Magnetic resonance (MR) tagging [1, 2] is a technique used to impose a known intensity pattern, called a tag pattern, on an object by spatially modulating the object's proton spin density before the image is acquired. Since the tag pattern moves with the object, MR tagging is particularly useful in the estimation of deformable motion from MR image sequences because some tag patterns can resolve motion ambiguities such as the aperture problem and improve the accuracy of optical flow motion estimates. In this paper we present an experimental validation of the tag pattern optimization method in [3, 4] in a practical MR imaging environment. This experiment includes a study of the effects of temporal sampling on the optimal frequency that was not done in [3, 4]. Our experimental results show that the tag pattern optimization method in [3, 4] is valid in a practical MR imaging application.

1. INTRODUCTION

Magnetic resonance (MR) tagging [1, 2] is a technique used to impose a known intensity pattern, called a tag pattern, on an object by spatially modulating the object's proton spin density before the image is acquired. A wide variety of tag patterns can be generated with this technique ranging from parallel line patterns [2] to sinusoidal patterns such as spatially modulated magnetization (SPAMM) [5]. Since the tag pattern moves with the object, MR tagging is particularly useful in the estimation of deformable motion from MR image sequences because some tag patterns can resolve motion ambiguities such as the aperture problem and improve the accuracy of optical flow motion estimates [6, 3, 4]. In these applications it is important to have a method for determining the optimal tag pattern a priori.

MR tagging was originally developed for cardiac motion analysis [1] and most of the research in this area has focussed on relatively high frequency starburst and parallel line tag patterns [2]. The motion of the tag lines can provide accurate measurements of the motion component orthogonal to the tag line. Only a relatively small portion of the object is tagged, however, resulting in a fairly sparse set of measurements. Prince and McVeigh proposed using low-frequency SPAMM tag patterns for motion estimation in [6] and used a modified version of Horn and Schunck's classical optical flow algorithm (HSOF) [7] to compute an estimate of the object's velocity field. Low-frequency tag patterns have the advantage of providing motion information at practically all pixels in the image. In addition, the relatively low bandwidth of these patterns makes it possible to acquire the images more quickly by reducing the number of frequency components that are sampled [2].

Prince and McVeigh's research in [6] also showed that the optical flow estimation error was dependent on the spatial frequency of the SPAMM pattern and, more importantly, an optimal frequency existed. Denney and Prince [3, 4] proposed a method for determining this optimal frequency a priori. Their method formulates HSOF as a stochastic linear smoother, and the estimation error covariance is shown to be Σ^{-1}, where Σ is matrix obtained by finite-differencing the estimate equation in [7]. The matrix Σ is a function of the tag pattern gradient and a measurement noise variance $\sigma_w^2(\omega)$ that models the effects of finite-differencing errors on the velocity estimate as a function of tag pattern frequency ω. The optimal tag pattern frequency is obtained by minimizing the average error covariance $p(\omega)$, which is proportional to the trace of Σ^{-1}. We call $p(\omega)$ the *parametric expected performance* (PEP). Simulation results in [3, 4] showed that use of the optimal frequency tag pattern results in a significant decrease in the estimation error relative to sub-optimal frequencies. Practical implementation of the methods in [3, 4], however, is complicated because in MR imaging phenomena other than motion, such as GRASS equilibrium artifacts and the T_1 relaxation of the tag pattern [1], can cause temporal intensity changes in the image sequence. These phenomena are difficult to model and cause consistent intensity changes that cannot be smoothed out of the motion estimate as is the case with random noise processes. In addition, the actual tag pattern applied to the object is a distorted version of the ideal because the object moves while the tag pattern is applied.

In this paper we present an experimental validation of the tag pattern optimization method in [3, 4] in a practical MR imaging environment. This experiment includes a study (not done in [3, 4]) of the effects of temporal sampling on the optimal frequency. A summary of the steps in our experiment is as follows:

1. A silicone gel phantom was constructed and mounted in a motor-driven apparatus that repetitively stretch-

This work was supported by the Whitaker Foundation of Mechanicsburg, PA.

0-8186-6950-0/94 $4.00

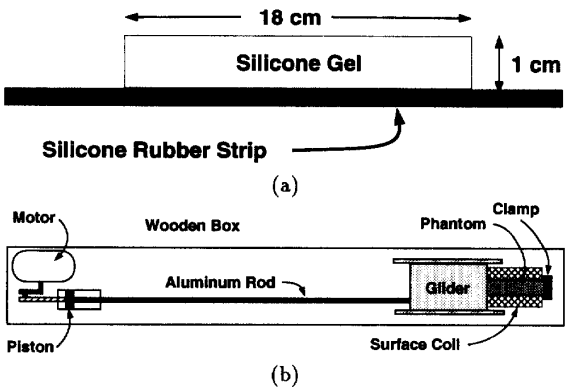

Figure 1: Experimental setup: (a) deformable phantom, (b) phantom deformation apparatus.

ed the phantom.

2. The deforming phantom was imaged in an MR scanner every 32.5ms with a 2D SPAMM tag pattern at thirteen different spatial frequencies.
3. The true velocity field was measured from high-resolution planar tagged image sequences of the phantom.
4. The theoretically optimal spatial frequency was determined using the method in [3, 4].
5. A velocity field was estimated from the first two images in each sequence using HSOF.
6. The HSOF estimation error versus spatial frequency was computed and compared to the theoretical result from Step 4.
7. The effects of temporal sampling on the optimal tag pattern were studied by repeating steps 4-6 for the first and third images in each sequence.

This paper is organized as follows. The details of steps 1—3 are presented in Sections 2—4 respectively. The details of steps 4—7 are presented in Section 5. Finally in Section 6 we summarize and discuss directions for future research.

2. EXPERIMENTAL SETUP

Our experiment setup consisted of two pieces of equipment: a deformable phantom and a motor-driven apparatus to repetitively stretch the phantom.

2.1. Deformable Phantom

The deformable phantom consisted of a 18cm long by 5cm wide by 1cm thick piece of silicone gel bonded to a strip of silicone rubber as shown in Figure 1a. The rubber strip was attached to the motor-driven apparatus described below and was repetitively stretched. The silicone gel moved with the rubber strip because of the bond. Silicone gel emits a high-strength signal when imaged in an MR scanner, and the silicone rubber base provided the mechanical strength needed to withstand repeated stretching. The bond was obtained by molding and curing the gel on the rubber strip. The gel was cured in a vacuum chamber to minimize the number and size of air bubbles in the gel. The silicone gel used in the phantom was Dow Corning Sylgard 527 Dielectric Gel, which comes in two parts: "A" and "B." This phantom consisted of 60ml of "A" and 70ml of "B."

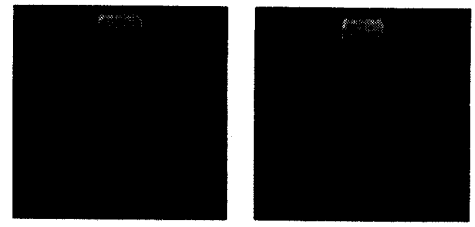

29ms 517ms

Figure 2: Untagged deforming phantom.

2.2. Motor-Driven Apparatus

The phantom was repetitively stretched by a motor driven apparatus mounted on a 19cm × 10cm × 45.8cm wooden box as shown in Figure 1b. This apparatus was also used in [8] to validate the accuracy of planar tags The motor is a Harvard Apparatus Model 607 respirator pump, which is configured to drive the piston in a cyclical motion. The phantom is mounted on the other end of the box and is connected to the motor by a hollow aluminum tube (1.9 cm outer diameter, 1.6mm thickness). This configuration isolates the ferromagnetic motor components from the scanner magnet. One end of the phantom's rubber strip is clamped to the wooden box, and the other end is attached to a glider mounted on a track with Teflon tape bearings. These bearings constrain the phantom motion to be along the length of the box. The pump was set to operate at 50 cycles/min. with a stroke length of 2cm.

3. IMAGING

The phantom end of the box was inserted into the bore of a GE Signa 1.5 Tesla MR scanner and imaged every 32.5ms with a fractional-echo segmented k-space imaging sequence [2]. The MR signal was detected with a standard surface coil mounted underneath the phantom as shown in Figure 1b. The imaging sequence was triggered by a cam mounted on the motor axle, which depressed a microswitch when the phantom was at its minimum stretch position. Two time frames of an untagged image sequence of the phantom are shown in Figure 2. Each image is 256 × 256 with a spatial resolution of 0.9375mm and pixel values in the range $[0, 65535]$.

The phantom was also imaged with a 1-1 SPAMM tag pattern [5] at the thirteen different spatial frequencies. The first and third images from two sequences with different spatial frequencies are shown in Figure 3.

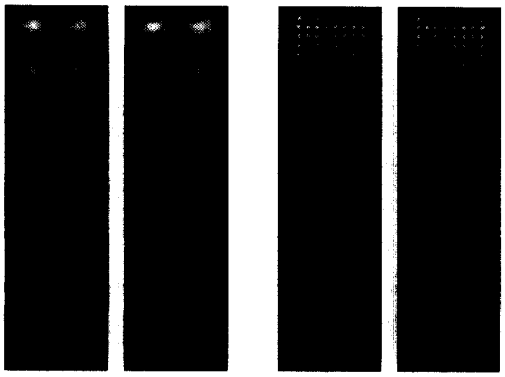

(a) (b)

Figure 3: First and third images in SPAMM tagged sequences: (a) 0.2 rad/mm, (b) 1.1 rad/mm.

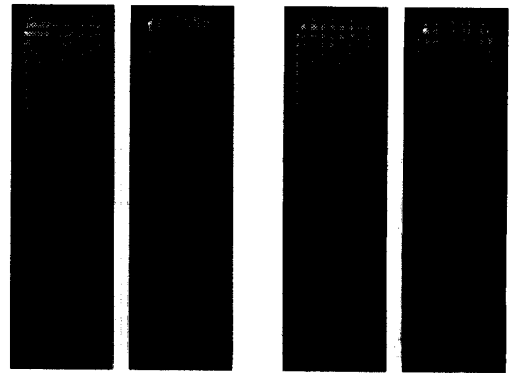

25ms 25ms 25ms 227ms
(a) (b) (c)

Figure 4: Planar tagged deforming phantom: (a) Horizontal tags (b) vertical tags. (c) composite image sequence.

4. TRUE VELOCITY FIELD

To determine the true velocity field, two planar tagged image sequences of the phantom were acquired with a temporal sampling interval of 6.5ms. In the first sequence, parallel tag planes were applied perpendicular to the direction of motion ("horizontal" tags) as shown in Figure 4a. In the second sequence, the tag planes were applied parallel to the direction of motion ("vertical" tags) as shown in Figure 4b. For each time frame, a composite image (Figure 4c) is formed from the horizontally and vertically tagged images with the following formula:

$$p_{ij}^{c} = \min(p_{ij}^{h}, p_{ij}^{v}),$$

where p_{ij}^{c}, p_{ij}^{h} and p_{ij}^{v} are the ijth pixel values for the composite, horizontal and vertical images respectively. The true velocity field of the phantom was determined at each tag line intersection by tracking the intersection through the composite image sequence. The procedure used to track the intersections and compute the true velocity field is summarized below. The details can be found in [9].

The tag line intersection points were located by separately identifying the tag line locations in the horizontally and vertically tagged images. For the horizontally tagged images, the data was read into a numerical software package column by column. For the vertically tagged images, the image was rotated 90 degrees and then read column by column. The intensity profile of the image was used to determine the approximate width of the phantom, and only those columns within this range were processed. To increase the signal to noise ratio, each column was averaged with its two nearest neighbors. The following steps were performed on each column in each image: 1) perform a 256-point fast Fourier transform (FFT) on the column, 2) low-pass filter the column with a Gaussian filter kernel, 3) zero-pad the column to 4096 points to achieve sub-pixel tag position resolution, 4) perform a 4096-point inverse FFT, 5) multiply the column by a normalizing function to correct for low-frequency intensity changes throughout the column and 6) detect local minima.

Once the tag lines were identified in both the vertically and horizontally tagged image sequences, the locations of intersection points were computed. The velocity of an intersection point between a given pair of time frames was computed by subtracting the intersection position in the first time frame from its position in the second time frame and dividing by the time interval between the two frames. This method was used to compute the true velocity field of the phantom at each tag line intersection in the composite image sequence.

5. TAG PATTERN OPTIMIZATION

In this section, we determine the a priori optimal spatial frequency ω for the SPAMM tag pattern using the method described in [3, 4] and compare the results with the actual error in HSOF velocity estimates. The major steps in this procedure are: 1) derive an analytical expression for the measurement noise variance $\sigma_w^2(\omega)$, 2) identify the parameters for the tag pattern, imaging environment and true velocity, and 3) compute the PEP $p(\omega)$ and actual HSOF estimation error for each of the thirteen spatial frequencies used to tag the phantom.

5.1. Measurement Noise Variance

The SPAMM tag pattern can be described by the following equation [6]

$$\psi(\mathbf{r}) = A(\cos^2\theta - \sin^2\theta\cos\omega r_x)(\cos^2\theta - \sin^2\theta\cos\omega r_y), \quad (1)$$

where A is the amplitude, $\theta = \xi_m \pi/2$ and $\xi_m \in [0, 1]$ is a parameter called the *tag modulation coefficient*. As in [3, 4], we assume that the tag pattern is randomly placed relative to the image frame. We model this uncertainty by making

the substitution

$$r_x = r_x + \phi_x$$
$$r_y = r_y + \phi_y$$

in (1), where ϕ_x and ϕ_y are independent random variables each uniformly distributed on a $2\pi \times 2\pi$ square. We further assume that each image is corrupted with zero mean additive white Gaussian noise with variance σ_a^2. With these assumptions, it can be shown that [9]

$$\sigma_w^2(\omega) = \tag{2}$$
$$\frac{2\sigma_a^2}{\Delta t^2} + \frac{\Delta t^2}{16} A^2 \omega^4 \sin^4\theta \times$$
$$[(v_{\max_x}^4 + v_{\max_y}^4)(2\cos^4\theta + \sin^4\theta) +$$
$$6\sin^4\theta v_{\max_x}^2 v_{\max_y}^2)], \tag{3}$$

where Δt is the temporal sampling interval and $\mathbf{v}_{\max} = [v_{\max_x}, v_{\max_y}]^T$ is the maximum velocity of the true velocity field.

5.2. Parameter Identification

Numerical values for the amplitude and tag pattern modulation coefficient were obtained from a manual inspection of the intensity values in the first image in each of the thirteen SPAMM tagged image sequence. It was observed that the intensity at the SPAMM pattern "peaks" varied by about 20% from the upper left corner (highest peak) of the phantom to the lower right corner (lowest peak) in a given image and also varied by about 10% between image sequences. The intensity of the SPAMM pattern "valleys" was observed to be fairly constant across both the phantom and the image sequences. The SPAMM pattern peaks occur at points where x and y satisfy $\cos\omega x = \cos\omega y = 1$, and the valleys occur when $\cos\omega x = \cos\omega y = -1$. Therefore, the amplitude and modulation coefficient can be computed from the peak and valley intensities by solving (cf. (1))

$$\begin{aligned} \psi_{\text{peak}} &= A(\cos^2\theta + \sin^2\theta)^2 \\ \psi_{\text{valley}} &= A(\cos^2\theta - \sin^2\theta)^2 . \end{aligned} \tag{4}$$

Equation (4) was solved numerically with $\psi_{\text{peak}} = 481.0$ and $\psi_{\text{valley}} = 64.0$. The ψ_{peak} value reflects an average across the phantom and across the image sequences. The resulting parameters are shown in Table 1.

The remainder of the parameters in Table 1 were determined as follows. The imaging noise variance σ_a^2 was chosen heuristically to account for the random receiver noise and other factors such as spatial variation in SPAMM pattern amplitude and tag pattern fade. The sampling intervals $\Delta t, \Delta x$ and Δy were derived from the image acquisition process. The lattice size $N_x \times N_y$ reflects the fact that the images in each sequence were cropped to contain only the phantom. The maximum velocity is determined from the position of the free end of the phantom in each image, and for this case, the motion was observed to be approximately three pixels or 43.0mm/sec. The velocity field smoothness parameter σ_u^2 was chosen empirically.

Parameter	Value
Amplitude (A)	481.0
Modulation Coefficient (ξ_m)	0.4575
Imaging Noise (σ_a^2)	2000.0
Temporal Sampling (Δt)	32.5ms
Spatial Sampling ($\Delta x = \Delta y$)	0.9375mm
Lattice Size ($N_x \times N_y$)	64 × 200
Maximum Velocity ($v_{\max_x} = v_{\max_y}$)	43.0mm/sec
Velocity Smoothness (σ_u^2)	5.0sec^{-1}

Table 1: Parameters for SPAMM tag pattern optimization.

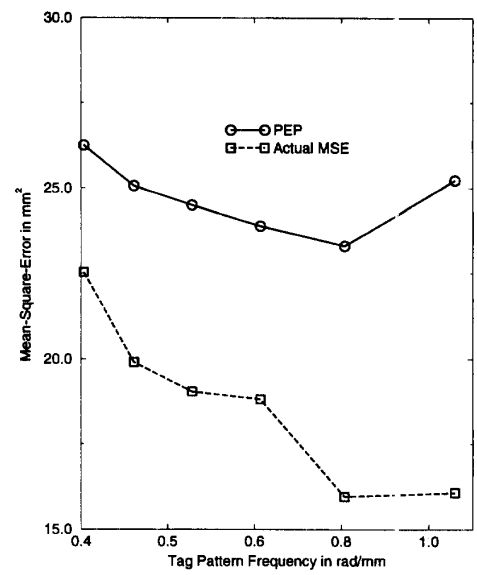

Figure 5: PEP and actual MSE versus spatial frequency for first and second images

5.3. Expected and Actual Performance

Equations (1) and (3) and the parameters in Table 1 were used to compute the PEP given by

$$p(\omega) = \frac{\sigma_u^2}{2N_x N_y} \text{tr}[\Sigma^{-1}] \tag{5}$$

for the thirteen spatial frequencies used to tag the phantom. As mentioned in [3, 4], computation of $p(\omega)$ for a given ω requires computing an average of the error variances over all points in the $N_x \times N_y$ lattice. In this experiment, we compute an average error variance only over a subset of lattice points to reduce the computation demand. This subset consisted of every other planar tag intersection point (see Figure 4c).

The PEP versus frequency for the first and second images in each sequence is plotted with a solid line in Figure 5. A velocity field estimate for each frequency was computed using HSOF with no compensation for the tag pattern fade.

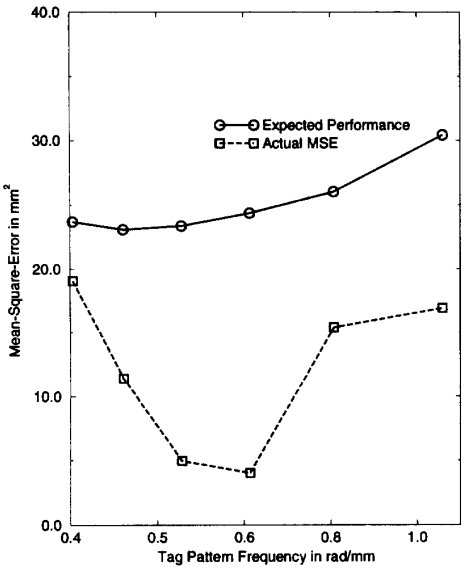

Figure 6: PEP and actual MSE versus spatial frequency for first and third images

The regularization parameter for each image pair was calculated using the formula [3, 4]

$$\alpha^2(\omega) = \sigma_u^2/\sigma_w^2(\omega).$$

The truth model described above was used to compute actual mean-square estimation error (MSE) at the same lattice points used to compute the PEP. The MSE versus spatial frequency is plotted with the dotted line in Figure 5. The PEP plot predicts an optimal spatial frequency of 0.79rad/mm, and the actual MSE is minimized at the same point. The offset and shape of these curves are different because the PEP is a measure of the estimation error averaged over all realizations of the random processes in the measurement and state models. Each point on the actual error curve is the estimation error for a particular realization.

The effect of temporal sampling on the optimal frequency was studied by considering the first and third images in each sequence. In this case the temporal sampling interval is 2×32.5ms $= 65.0$ms with approximately the same maximum velocity. The PEP and actual MSE versus frequency is shown in Figure 6. The PEP curve predicts that doubling the temporal sampling period shifts the optimal frequency to 0.45rad/mm while the actual MSE is minimized at 0.63rad/mm. A possible reason for this discrepancy is that the spurious intensity changes due to phenomena such a tag pattern fade become more significant at longer temporal sampling intervals.

6. DISCUSSION

Our experimental results show that the tag pattern optimization method in [3, 4] are valid in a practical MR imaging application. The differences between the actual and predicted optimal frequency can be attributed to the unmodeled noise processes such as GRASS equilibrium artifacts and tag pattern fade and errors in the approximate method for computing the a priori optimal frequency. A technique for compensating for the T_1 fade was proposed in [6], but this method makes the fairly restrictive assumption that the spatial distribution of the object's T_1, T_2 and proton density is known a priori. In future work we plan to propose less restrictive methods of compensating for tag fade and equilibrium artifacts.

7. REFERENCES

[1] E.A. Zerhouni, D.M. Parish, W.J. Rogers, A. Yangand, and E .P. Shapiro. Human heart: tagging with MR imaging — a method for noninvasive assessment of myocardial motion. *Radiology*, 169:59–63, 1988.

[2] E. R. McVeigh and E. Atalar. Cardiac tagging with breath-hold cine MRI. *Magnetic Resonance in Medicine*, 28:318–327, 1992.

[3] T.S. Denney Jr. and J.L. Prince. Optimal brightness functions for 2-D optical flow. In *Proc. of the IEEE Int'l Conf. Acoustics, Speech, and Signal Processing*, pages V225—V228, Minneapolis, MN, April 1993.

[4] T.S. Denney Jr. and J.L. Prince. Optimal brightness functions for optical flow estimation of deformable motion. *IEEE Transactions on Image Processing*, 3(2):178—191, March 1994.

[5] L. Axel and L. Dougherty. MR imaging of motion with spatial modulation of magnetization. *Radiology*, 171:841–845, 1989.

[6] J.L. Prince and E.R. McVeigh. Motion estimation from tagged MR image sequences. *IEEE Transactions on Medical Imaging*, 11(2):238—249, June 1992.

[7] B.K.P. Horn and B.G. Schunck. Determining optical flow. *Artificial Intelligence*, 17:185–203, 1981.

[8] C. C. Moore, S. B. Reeder, and E. R. McVeigh Tagged MR imaging in a deforming phantom: photographic validation. *Radiology*, 190:765—769, 1994.

[9] T.S. Denney Jr. *Stochastic estimation of deformable motion from magnetic resonance tagged cardiac images.* PhD thesis, The Johns Hopkins University, 1994.